Polarization tuning of an *H*1 organic-inorganic nano-cavity

Mohamed M. Murshidy[1], Ali M. Adawi[2] , Paul W. Fry[3] and David G. Lidzey[4,a]

[1]Department of Physics, College of Applied and Supporting Studies, King Fahd University of Petroleum and Minerals, Dhahran 31261, Saudi Arabia

[2]Department of Physics and Mathematics, University of Hull, Cottingham Road, Hull, HU6 7RX, United Kingdom

[3]Nanoscience and Technology Centre, University of Sheffield, North Campus, Broad Lane, Sheffield, S3 7HQ, United Kingdom

[4]Department of Physics and Astronomy, The University of Sheffield, Hicks Building, Hounsfield Road, Sheffield S3 7RH, United Kingdom

[a]Author to whom correspondence should be addressed: d.g.lidzey@sheffield.ac.uk

ABSTRACT

We investigate the optical properties of the dipole-like modes of an *H*1 nano-cavity consisting of a single missing air hole imbedded into a triangular two-dimensional silicon nitride (Si_3N_4) based photonic crystal coated with a red-fluorescent molecular dye. We modify the size and position of the first six neighboring air holes around the nano-cavity and demonstrate that this allows a control over the energy and separation of two dipole-like optical modes (M_x and M_y). This allows us to produce either linearly polarized optical modes or an unpolarized optical mode composed of degenerate modes having orthogonal polarization. We confirm our findings using three-dimensional finite difference time domain (FDTD) calculations.

I. INTRODUCTION

A photonic crystal nano-cavity is a structure in which a physical defect is deliberately introduced in an otherwise perfect photonic crystal[1-3]. In such a structure, light of certain frequencies can become trapped in the defect, with the volume of the cavity being around $(\lambda/n)^3$ [4-7]. Such properties make photonic crystal nano-cavities very attractive systems to study light matter interaction at the nanoscale in both weak [8,9] and strong coupling regimes [10,11]. Photonic crystal nano-cavities have been explored for applications as single photon sources [12,13], sensor devices [14] and quantum cryptography systems.[15,16] Here applications require a close control over the polarization state of the cavity mode; for example in quantum cryptography, an unpolarized optical cavity mode is desirable [17], whilst single photon light sources generally require a linearly polarized optical mode [18].

Families of different 2D-photonic-crystal nano-cavities have been explored in which a physical defect is created from a linear array of missing holes in a triangular lattice, with cavities created from 3, 5 and 7 missing holes referred to as L3, L5 and L7 cavities [19-21]. Here, larger cavities generally have a higher quality-factor (Q-factor) with this parameter being important in applications such as low-threshold lasers [22,23]. However, the optical mode volume (V) of a cavity is also of importance as the Q/V ratio defines the Purcell Factor (enhancement of spontaneous emission rate) that occurs when placing an emitter into the cavity, with large spontaneous emission rates being of importance in single-photon light sources[24,25]. To combine both large Q and small V, researchers have explored so-called $H1$ nano-cavities that are created by defining a single missing air hole defect into a two-dimensional triangular lattice photonic crystal slab [26-28]. Here a number of different types of $H1$ structures have been created using materials of different refractive index. For example, cavities have been realized based on materials having a high refractive index ($n = 3.46$) with a maximum (measured) Q-factor determined of around 10^6 based on a structure having a slab thickness $d = 0.575a$ [27]. By using a dielectric material of lower refractive index ($n = 1.93$) it has been predicted [29] that the Q-factor is expected to reduce to around 700 based on a slab-thickness of $1.55a$. Q-factor can however be enhanced by modifying the size and position of the first six nearest-neighboring air-holes that surround the nano-cavity defect [28,30].

In this work we present a modelling and experimental study of the polarization state of an $H1$ nano-cavity that is coated with a red-emitting molecular dye (see Fig. 1 (a)). It is known that an $H1$ nano-cavity will support a degenerate dipole-like optical mode that in fact corresponds to two modes having the same frequency but with different polarizations [28,31,32]. Here we demonstrate that the Q-factor of an $H1$ nano-cavity can be enhanced and the polarization state of the cavity mode controlled [4,28,30] by reducing the symmetry of the surrounding holes in the photonic crystal. This reduction in symmetry is realized via modifying the size and position of the first six neighboring air holes that surround the nano-cavity 'missing hole'. We then demonstrate that the degeneracy of the cavity mode can be removed by reducing the structure symmetry, allowing us to tune the polarization of the cavity mode from being x-polarized to y-polarized or into an unpolarized state. Our cavities are constructed using the dielectric material silicon nitride (Si_3N_4) which is coated with a thin film of the molecular dye Lumogen Red, allowing the dipole-like mode to be positioned at optical frequencies (650 – 670 nm). We show that our modified cavities can reach a Q-factor of 1875; a value that is almost one order of magnitude compared to an unmodified $H1$ cavity.
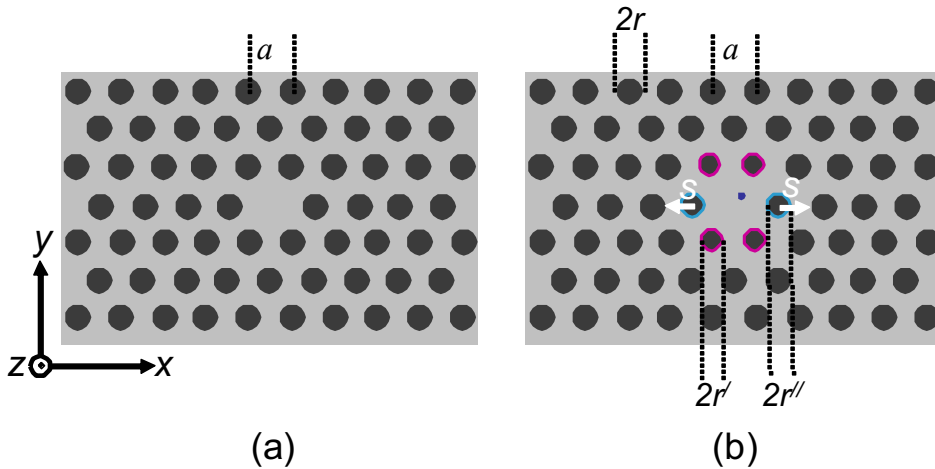
FIG. 1. (a) A schematic diagram of a single missing air hole nano-cavity. (b) A schematic diagram of the location and layout of the holes that surround the nano-cavity explored in this work. The blue dot in Fig. 1(b) represents the location of the dipole emitter used in the FDTD simulations which is displaced 10 nm from the cavity centre in both x and y-directions

II. MODELING

The structure of the nano-cavities investigated in this work are shown in Fig. 1. This structure is based on a single missing air hole cavity in a triangular two-dimensional Si_3N_4 photonic crystal membrane having a refractive index $n = 2.1$, thickness $d = 200$ nm, lattice constant of $a = 260$ nm and a hole radius $r = 0.3a$. Here the value of r was chosen based on the results from previous reported studies as it allows a TE band-gap to be

created in such photonic crystal devices [26,33-35]. To improve the cavity quality factor and control its polarization state, we have reduced the size of the first two air holes above and below the cavity (parallel to the x-axis) to $r' = 0.23a$. The size of the air holes neighboring the cavity were also reduced to $r'' = 0.26a$ and they were displaced by a distance s away from their original position. We chose the values of r' and r'' based on the fabrication capability and resolution of our electron beam lithography (EBL) system, with $r - r'' = 10\ nm$ and $r'' - r' = 8\ nm$. As we show below, this lowering of cavity symmetry created by reducing the size of the first two air holes above and below the nano-cavity breaks the degeneracy of the cavity mode and splits it into two linearly polarized modes M_x and M_y.

We have used three-dimensional finite time difference time domain (FDTD) calculations to investigate the optical properties of our nano-cavities. [36] Here, the photonic crystal size was set to be $34a \times 19\sqrt{3}a$ with boundary conditions implemented by introducing a perfect matching layer around the structure. The Q-factor was calculated by imbedding an oscillating dipole emitter of a dipole moment $P(x, y, z) = (1,1,0)$ at a weak symmetry point that was 10 nm away from the cavity centre. Here, the dipole source was modelled as a Gaussian oscillating pulse centred at 628 nm with a linewidth of 100 nm. The Poynting vector leaving the cavity was then calculated, with emission from a single dipole emitter being sufficient to study the dependence
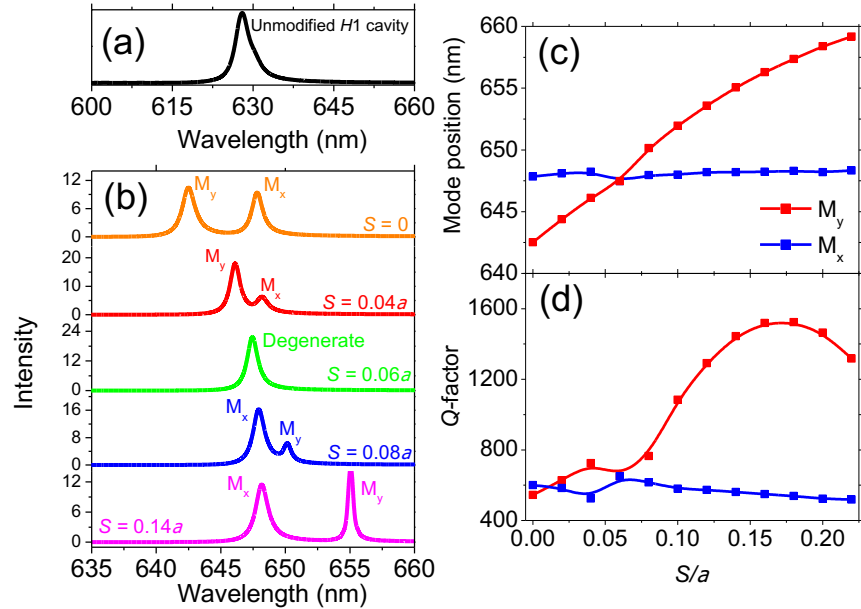
FIG. 2. (a) FDTD simulated emission spectrum of an unmodified H1 nano-cavity. (b) The FDTD simulated emission spectra of a modified H1 nano-cavity as a function of displacement (s) of the side air-holes in a direction corresponding to the x-axis. (c) The position of mode M_x and M_y as a function of s. (d) The Q-factor of modes M_x and M_y as a function of the side-air holes displacement s. In all these calculations, $a = 260nm, d = 200nm, r = 0.3a, r' = 0.23a, r'' = 0.26a$ and $n = 2.1$.

of the *Q*-factor and mode shift on the displacement (*s*) of the side air-holes. Here, the cavity *Q*-factor of the structures was calculated by relating the cavity emission linewidth at half maximum $\Delta\lambda$ to the wavelength of the cavity mode λ via $Q = \Delta\lambda/\lambda$.

In Fig. 2(a) we plot the FDTD simulated emission spectrum for an unmodified *H*1 nano-cavity (i.e. *r* = 0.3a, *s* = 0). Our calculations also indicate that this mode is a dipole-like cavity mode composed of two degenerate modes having orthogonal polarization. We find as expected that by reducing the symmetry of the *H*1 nano-cavity (realised by either modifying the size of the air-holes that surround the cavity or by displacing the side air-holes) we create a splitting of cavity mode into two modes having orthogonal polarizations. This is shown in Fig. 2(b), where we plot a series of simulated emission spectra for an *H*1 nano-cavity having air hole size $r = 0.3a, r' = 0.23a, r'' = 0.26a$ and different side-hole shift *s*, where holes have been displaced in a direction parallel to the *x*-axis. Here the cavity symmetry is broken through changed hole size (i.e. $r \neq r' \neq r''$) and we find that the cavity supports two optical modes labelled M_x and M_y which are defined by their polarization direction. Fig. 2(c) and 2(d) plot the calculated wavelength and *Q*-factor of modes M_x and M_y respectively as a function of side-hole shift.

Our calculations (see Fig. 2(b)) indicate that mode M_x is sensitive to modification of the size of the surrounding air-holes and causes it to undergo a red-shift from 628 nm to 648 nm as air-hole size is reduced from 78 nm to 59.8 nm for the first two air holes above and below the cavity (r') and from 78 nm to 67.6 nm for air holes neighboring the cavity (r'') . This red-shift is accompanied by an increase in cavity *Q*-factor from 200 to 650. Interestingly however, we find (see Fig. 2(c) and (d)) that the *Q*-factor and wavelength of mode M_x is not apparently dependent on the air-hole side-shift *s*. In contrast, the *Q*-factor and wavelength position of mode M_y has a strong dependence on *s*. Indeed, it can be seen that mode M_y undergoes a 17 nm shift to longer wavelengths as *s* is increased from *s* = 0 to 0.22*a*; a result that we ascribe to an increase in the physical volume of the nano-cavity.

As can be seen in Fig 2(b), our model indicates that mode M_y undergoes a spectral overlap with mode M_x at $s = 0.06a$ forming a degenerate state. It is apparent that the total integrated area under the peaks of both M_x and M_y is almost constant, however when such modes are close in energy, we see a transfer of area between them. If we simplistically equate the total area of the emission peaks with the amount of energy stored within the cavity, it suggests an effective transfer of electromagnetic energy stored in each mode as they approach degeneracy[37]. Fig. 2(d) also reveals that the *Q*-factor of mode M_y has a strong dependence on shifting the side-

holes in the x-direction, with a maximum value of 1,500 predicted for $s = 0.18a$; a value almost 8 times higher than the Q-factor of the unmodified cavity. We attribute this increase in Q-factor to a reduction of radiation

losses from guided modes due to the gentle confinement of the field that occurs as a result of the modifications to the cavity structure [4].
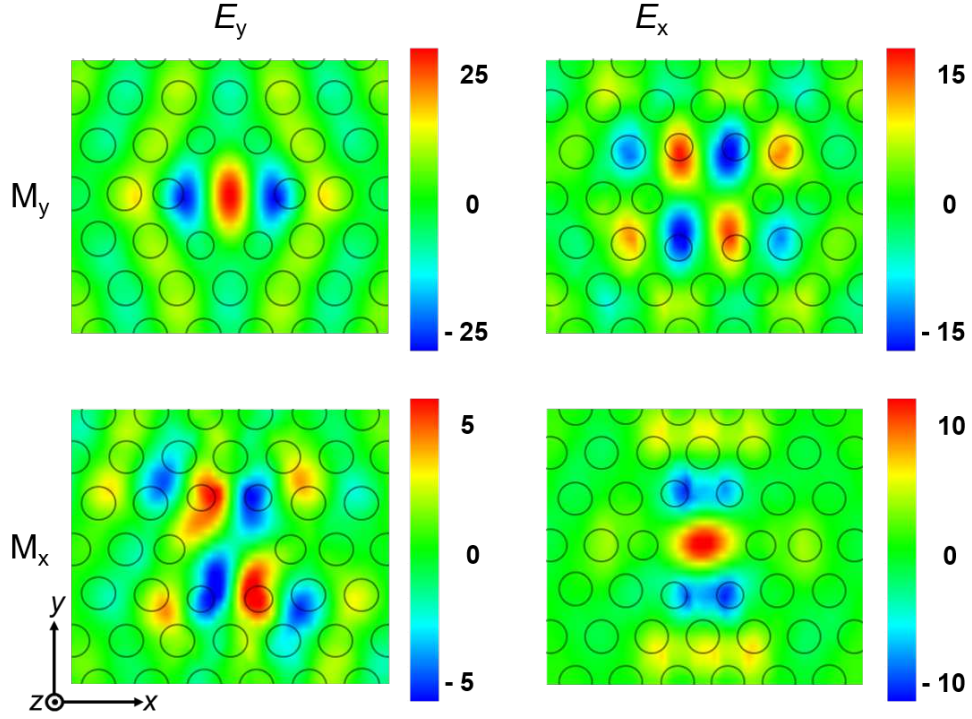

FIG. 3. Electric field distributions at the cavity centre at wavelengths corresponding to modes M_y and M_x at $s = 0.14a$.

In order to gain further insight into the optical modes identified in Fig. 2, we have calculated the electromagnetic field distribution associated with mode M_y and M_x respectively. The results of these calculations are plotted in Fig. 3 for $s = 0.14a$. Here it is apparent that both modes M_x and M_y have a dipole-like field distribution[26,38]. We can use this calculated field distribution to explain the finding (see Fig. 2(c) and (d)) that mode M_y appears most sensitive to changes in displacements of the side holes in the x-direction position, with such changes not apparently affecting mode M_x. It is clear that this sensitivity results from the fact that the E_y component of the M_y mode electric field distribution is oriented parallel to the x-direction (see Fig. 3). In contrast, it is apparent that the E_x component of the M_x field distribution will be most sensitive to modifications of the upper and lower air-holes (i.e. resulting from structure changes in the y-direction).

III. EXPERIMENTAL RESULTS AND DISCUSSION

To explore the results of our FDTD calculations, we fabricated a series of $H1$ nano-cavities having a lattice constant $a = 260\ nm$, air-hole radius $r = 75\ nm$, $r' = 60\ nm\ and\ r'' = 68\ nm$ into a pre-etched free standing Si_3N_4 membrane of thickness $200\ nm$ and refractive index $n = 2.1$. Cavities were created using electron beam lithography and reactive ion etching techniques. Here, cavities were fabricated into free-standing Si_3N_4 membranes purchased from Silson Ltd. The reader is directed to our previous papers that fully describe the lithography and patterning methods used [39,40]. Here, we used such techniques to fabricate a series of
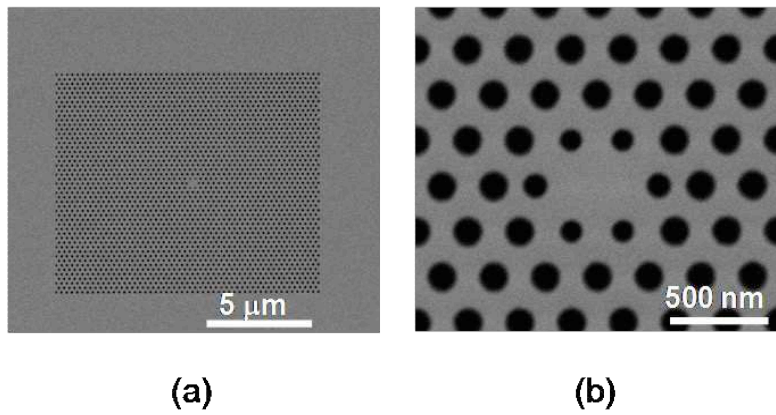

FIG. 4. Parts (a) and (b) show SEM images of a Si_3N_4-based $H1$ photonic crystal nano-cavity recorded at two different magnifications.

different photonic crystal nano-cavities into Si_3N_4 membranes, including regular L3, modified L3 and a 1-D photonic crystal nano-cavity [39-41].

Fig. 4(a) and (b) shows scanning electron microscope images recorded at two different magnifications of the nano-cavities fabricated. Following fabrication, a 3 nm thick layer of the molecular dye Lumogen Red was coated onto the cavity surface via thermal evaporation. Here, our previous work has confirmed that characterizing the fluorescence generated by such an organic surface-layer is an effective method to probe the optical structure of a photonic crystal nano-cavity [39].

Such structures were studied by generating photoluminescence (PL) using the 442 nm line of a HeCd laser. Here, the laser was focussed onto the sample to a 2500 μm^2 spot having an excitation power density of

15 W cm^{-2}, with the laser incident on the surface at an angle of 45° relative to the surface normal (so-called "dark field" configuration). The resultant PL was collected from the cavity surface at normal incidence using
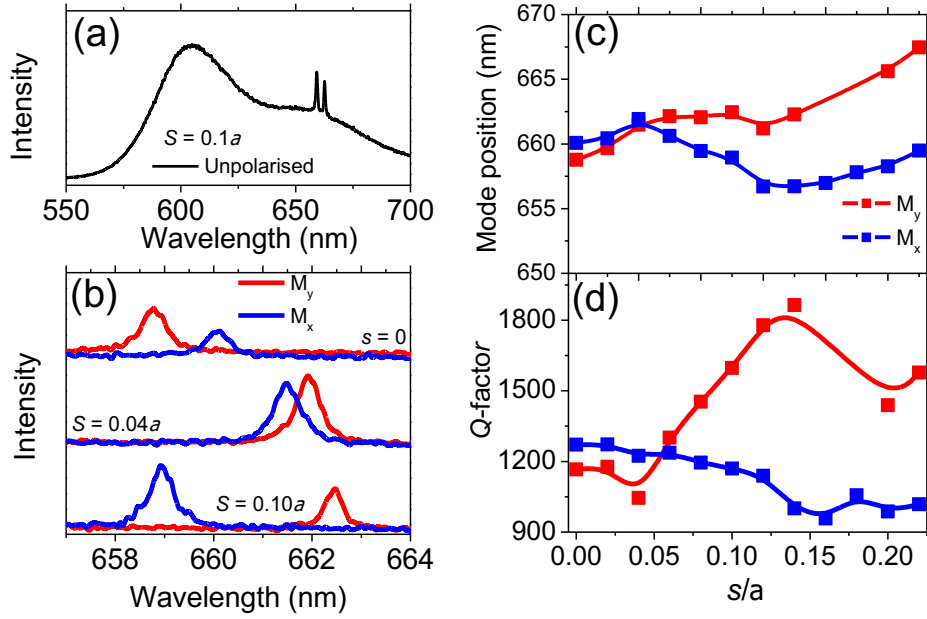

FIG. 5. (a) The fluorescence emission of unpolarized fluorescence emission of the Lumogen Red when coated onto a modified H1 nano-cavity surface. (b) Measured emission spectra of modified H1 nano-cavity as a function of the side air hole displacement s. (c) The measured spectral position of mode M_x and M_y as a function of s. (d) The measured Q-factor of M_x and M_y as a function of the side air hole displacement s.

a 50X objective lens with numerical aperture of 0.42. To reject plasma lines from the laser output, a long pass filter having a cut-off at 450 nm was placed just after the objective lens. The PL was then passed through an optical-polarizer oriented either parallel or perpendicular to the cavity x-axis before being imaged into a 0.25 m liquid nitrogen cooled CCD spectrometer. To separate the nano-cavity emission from that of the surrounding region, the spectrometer slit width was reduced to 0.01 mm, with data recorded from the rows that correspond to the cavity image on the CCD.

Fig. 5(a) shows a typical unpolarized PL emission spectrum measured from a modified H1 nano-cavity coated with Lumogen Red having a hole size $r = 0.3a, r' = 0.23a, r'' = 0.26a$ where a = 260 nm (see Fig. 1(b)). As it can be seen, the nano-cavity supports two optical modes. In order to characterise these modes in more detail, the PL emission was measured as a function of the cavity side air-hole shift s and emission polarization (selecting either M_x or M_y modes) - see typical emission spectra in Fig. 5(b). For the cavity having $s = 0$, the structure is characterised by two optical modes which we identify as M_x and M_y with $\lambda_{Mx} > \lambda_{My}$. Such findings are in good agreement with the FDTD calculations presented in Fig. 2(b). Note that we observe

small changes in the wavelength of mode M_x as a function of changing s (see Fig. 5(c)); a result most probably caused by uncontrolled variations in the structure of the photonic crystal, rather than from changes in s. Encouragingly we find that as s increases, mode M_y shifts to longer wavelengths as expected. Furthermore, the intensity of the emission peaks become comparable around $s = 0.04a$ indicating the formation of a near degenerate unpolarized state.

In Fig. 5(d) we plot the experimentally determined Q-factor of modes M_x and M_y as a function of s. Here, the cavity Q-factor was deduced by fitting the cavity mode emission to a Lorentzian function. As it can be seen, the Q-factor of mode M_x is approximately constant as a function of s. However, the Q-factor of mode M_y has a clear dependence on s and takes a maximum value of 1875 at $s = 0.14a$; a result in close agreement with our FDTD simulations as presented in Fig. 2(d). Here it can be seen that the measured Q-factor is slightly higher than the simulated Q-factor; an effect that we again attribute to structural differences between the modelled and fabricated structures.

IV. CONCLUSIONS

In summary, we have fabricated and modelled the optical properties of the dipole-like mode of a H1 silicon nitride nano-cavity that is coated with a red-fluorescent molecular dye. By modifying the size and position of the six air-holes surrounding the cavity, we showed that the Q-factor of a dipole-like mode can be enhanced by almost an order of magnitude compared to an unmodified H1 cavity. We also confirm that it is possible to manipulate the polarization and the energy separation between the dipole-like cavity modes, with the cavity either characterised by spectrally separate modes having orthogonal polarization, or a single unpolarized mode.

DATA AVAILABILITY

The data that support the findings of this study are available from the corresponding author upon reasonable request.

REFERENCES

[1]   B.-S. Song, S. Noda, and T. Asano, Science **300,** 1537 (2003).

[2]   J. D. Joannopoulos, S. G. Johnson, J. N. Winn, and R. D. Meade, *Photonic Crystals: Molding the Flow of Light* (Princeton University Press, 2008).

[3]   Y. Takahashi, Y. Tanaka, H. Hagino, T. Sugiya, Y. Sato, T. Asano, and S. Noda, Optics Express **17,** 18093 (2009).

[4]   Y. Akahane, T. Asano, B.-S. Song, and S. Noda, Nature **425,** 944 (2003).

[5]   K. Kuruma, Y. Ota, M. Kakuda, S. Iwamoto, and Y. Arakawa, Applied Physics Letters Photonics **5,** 046106 (2020).

[6]   Y. H. Ra, R. T. Rashid, X. Liu, J. Lee, and Z. Mi, Advanced Functional Materials **27,** 1702364 (2017).

[7]   M. Li, H. Liang, R. Luo, Y. He, J. Ling, and Q. Lin, Optica **6,** 860 (2019).

[8]   R. Wang, M. Ikezawa, Y. Sakuma, H. Takeda, N. Ikeda, Y. Sugimoto, K. Sakoda, Y. Yamada, and Y. Masumoto, ACS Photonics **7,** 321 (2020).

[9]   N. Takemura, M. Takiguchi, E. Kuramochi, A. Shinya, T. Sato, K. Takeda, S. Matsuo, and M. Notomi, Physical Review A **99,** 053820 (2019).

[10]   D. Dovzhenko, S. Ryabchuk, Y. P. Rakovich, and I. Nabiev, Nanoscale **10,** 3589 (2018).

[11]   P. M. Vora, A. S. Bracker, S. G. Carter, M. Kim, C. S. Kim, and D. Gammon, Physical Review B **99,** 165420 (2019).

[12]   P. Senellart, G. Solomon, and A. White, Nature Nanotechnology **12,** 1026 (2017).

[13]   Y. Wei, T. Zhao, B. Yao, R. Su, Y. Yu, J. Liu, and X. Wang, Optical Materials Express **10,** 170 (2020).

[14]   Y. Song, J. Bai, R. Zhang, E. Wu, J. Wang, S. Li, B. Ning, M. Wang, Z. Gao, and Y. Peng, Sensors and Actuators B: Chemical **310,** 127671 (2020).

[15]   N. Matsuda and H. Takesue, Nanophotonics **5,** 440 (2016).

16   Y. Li, X. Zhou, Q. Yang, Y. Li, W. Li, H. Li, S. Chen, M. Li, and Y. Song, Journal of Materials Chemistry C **5,** 4621 (2017).

17   T. Stace, G. J. Milburn, and C. Barnes, Physical Review B **67,** 085317 (2003).

18   W.-H. Chang, W.-Y. Chen, H.-S. Chang, T.-P. Hsieh, J.-I. Chyi, and T.-M. Hsu, Physical Review Letters **96,** 117401 (2006).

19   E. Kuramochi, E. Grossman, K. Nozaki, K. Takeda, A. Shinya, H. Taniyama, and M. J. O. l. Notomi, Optics Letters **39,** 5780 (2014).

20   S. L. Portalupi, M. Galli, C. Reardon, T. Krauss, L. O'Faolain, L. C. Andreani, and D. J. O. e. Gerace, Optics Express **18,** 16064 (2010).

21   A. M. Adawi, A. R. A. Chalcraft, D. M. Whittaker, and D. G. Lidzey, Optics Express **15,** 14299 (2007).

22   Y. Ota, K. Watanabe, S. Iwamoto, and Y. J. O. E. Arakawa, Optics Express **21,** 19778 (2013).

23   W. Xue, Y. Yu, L. Ottaviano, Y. Chen, E. Semenova, K. Yvind, and J. J. P. r. l. Mork, Physical Review Letters **116,** 063901 (2016).

24   J. Canet-Ferrer, L. J. Martínez, I. Prieto, B. Alén, G. Muñoz-Matutano, D. Fuster, Y. González, M. L. Dotor, L. González, P. A. Postigo, and J. P. Martínez-Pastor, Optics Express **20,** 7901 (2012).

25   J. Riedrich-Möller, S. Pezzagna, J. Meijer, C. Pauly, F. Mücklich, M. Markham, A. M. Edmonds, and C. Becher, Applied Physics Letters **106,** 221103 (2015).

26   J. Hagemeier, C. Bonato, T.-A. Truong, H. Kim, G. J. Beirne, M. Bakker, M. P. van Exter, Y. Luo, P. Petroff, and D. Bouwmeester, Optics Express **20,** 24714 (2012).

27   E. Kuramochi, H. Duprez, J. Kim, M. Takiguchi, K. Takeda, T. Fujii, K. Nozaki, A. Shinya, H. Sumikura, and H. Taniyama, Optics express **26,** 26598 (2018).

28   H. Takagi, Y. Ota, N. Kumagai, S. Ishida, S. Iwamoto, and Y. Arakawa, Applied Physics Express **10,** 062002 (2017).

29   F. Pisanello, A. Qualtieri, T. Stomeo, L. Martiradonna, R. Cingolani, A. Bramati, and M. De Vittorio, Optics letters **35,** 1509 (2010).

30   L. Kassa-Baghdouche and E. Cassan, Optical and Quantum Electronics **52** (2020).

31   M. Minkov and V. Savona, Scientific reports **4,** 5124 (2014).

32   I. Luxmoore, E. D. Ahmadi, B. Luxmoore, N. Wasley, A. Tartakovskii, M. Hugues, M. Skolnick, and A. Fox, Applied Physics Letters **100,** 121116 (2012).

33   H. Takagi, Y. Ota, N. Kumagai, S. Ishida, S. Iwamoto, and Y. Arakawa, Optics express **20,** 28292 (2012).

34   D. Englund, D. Fattal, E. Waks, G. Solomon, B. Zhang, T. Nakaoka, Y. Arakawa, Y. Yamamoto, and J. Vučković, Physical review letters **95,** 013904 (2005).

35   I. J. Luxmoore, E. D. Ahmadi, A. M. Fox, M. Hugues, and M. S. Skolnick, Applied Physics Letters **98,** 041101 (2011).

36   The 3D FDTD code (CrystalWave) used in this work is a product of Photon Design Ltd, (http://www.photond.com).

37   J. D. Jackson, *Classical Electrodynamics, Chapter 8* (Wiley, New York, 1962).

38   A. C. Thijssen, M. J. Cryan, J. G. Rarity, and R. Oulton, Optics express **20,** 22412 (2012).

39   A. M. Adawi, M. M. Murshidy, P. W. Fry, and D. G. Lidzey, ACS Nano **4,** 3039 (2010).

40   M. M. Murshidy, A. M. Adawi, P. W. Fry, and D. G. Lidzey, Applied Physics Letters **97,** 224 (2010).

41   M. M. Murshidy, A. M. Adawi, P. W. Fry, D. M. Whittaker, and D. G. Lidzey, Journal of the Optical Society of America B **27,** 215 (2010).